

Real-time detection, control, and sorting of microfluidic droplets

Xize Niu, Mengying Zhang, Suili Peng, Weijia Wen,^{a)} and Ping Sheng
Department of Physics and Institute of Nano Science and Technology, The Hong Kong University of Science and Technology, Clear Water Bay, Kowloon, Hong Kong

(Received 29 August 2007; accepted 18 September 2007; published online 3 October 2007)

We report the design and implementation of capacitive detection and control of microfluidic droplets in microfluidic devices. Integrated microfluidic chip(s) with detection/control circuit enables us to monitor *in situ* the individual volume of droplets, ranging from nanoliter to picoliter, velocity and even composition, with an operation frequency of several kilohertz. Through electronic feedback, we are able to easily count, sort, and direct the microfluidic droplets. Potential applications of this approach can be employed in the areas of biomicrofluidic processing, micro-chemical reactions as well as digital microfluidics. © 2007 American Institute of Physics. [DOI: [10.1063/1.2795392](https://doi.org/10.1063/1.2795392)]

I. INTRODUCTION

Droplets in miniaturized microfluidic systems have received much focused attention recently.¹⁻⁵ Chemical reactions and biotesting can benefit from many advantages afforded by the tiny droplets, ranging from nano- to picoliters in volume. Mixing of liquids is much easier in droplets than in continuous microflows.⁶ For biosensing/testing, accurate control can be achieved by conveying reagents in discrete volumes in the forms of droplets, which also allows single cell manipulations, as well as better statistics. Multiple emulsions⁷ or structured drops⁸ can offer even more functionalities, such as polymerization processing and encapsulation of droplets for targeted delivery and release.

Generation and manipulation of droplets involve discontinuous pressure changes, e.g., during droplet fusion and/or fission or the droplet formation process from the continuous phase.⁹⁻¹³ Drop size and distance may vary spatially and temporally. Hence, real time detection of droplets is critical for accurate control. Up to now, optical detection methods are the most widely used,^{14,15} e.g., using either photodiode for simple counting or high speed charge-coupled device (CCD) camera with image processing for detection of more detailed characteristics.

In this paper, we report the design and implementation of capacitive detection and control of microfluidic droplets in microchannels. Capacitive sensors are common in the MEMS community, widely used in acceleration and pressure sensing.^{16,17} In biosensing, Coulter counter has been used for counting and sizing particles and/or cells.^{18,19} Capacitive sensor was used to detect the electrical trapping of yeast cells onto gold electrodes in a microfluidic channel.²⁰ Capacitive cytometry²¹ was also used in measuring the DNA content in biological cells. Our approach differs from those mentioned above. By installing a pair of parallel electrodes across the microfluidic channel, very small variations in the capacitance can be detected when a droplet passes through. Due to the electrode's design and feedback electronic circuit, real-time and accurate determination of size, shape, and composition of droplets (with volumes ranging from pico- to nanoliter) has been demonstrated. The operational frequency can reach up to 10 kHz, a speed which is difficult to realize by conventional optical means. Thus, capacitive measurement of droplets has the

^{a)}Corresponding author. Electronic mail: phwen@ust.hk

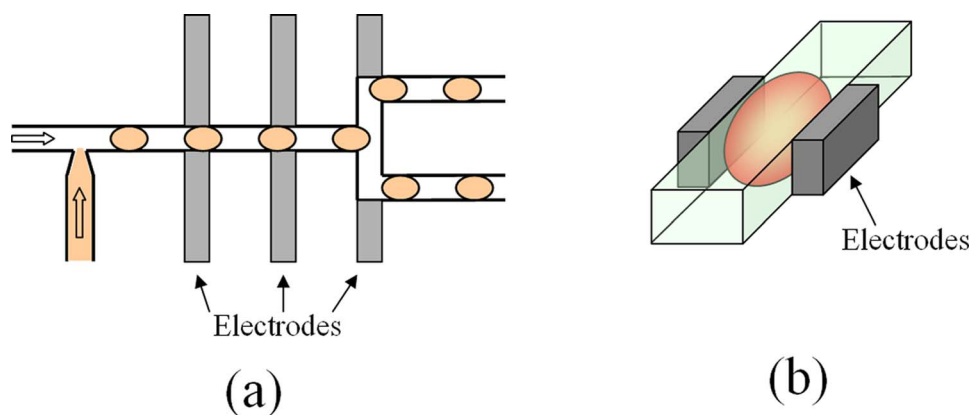


FIG. 1. (a) Schematic view of the microfluidic chip, with a T-shaped inlet to generate aqueous droplets and three pairs of coplanar electrodes along the main flow channel for detection and control. The two branches in the downstream are for droplet sorting. (b) A schematic 3-dimensional view of the capacitive droplet detection area.

potential to be simple, fast, and less expensive than the standard laser flow cytometry. Moreover, it can be used in portable lab-chips for *in situ* detection and control of droplets.

II. MATERIALS, METHODS, AND EXPERIMENTAL SETUP

A. Microfluidic chip

A microfluidic chip, as shown in Fig. 1(a), has a main flow channel on which several pairs of parallel electrodes are located. Two (or more) inlet channels, carrying two (or more) immiscible liquids, in which one is the carrying liquid and the other is for generating the droplets, are merged at the inlet junction. The droplets with the carrying stream are shown to flow through several pairs of electrodes intended for detection and manipulation.

Parallel electrodes are located on the side walls of the channel(s). Capacitance change is induced when a droplet passes through a pair of electrodes [shown schematically in 1(b)], owing to the dielectric constant contrast between the droplet and the carrying fluid. Thus dielectric constant difference between the two liquids is a prerequisite for capacitive sensing, but this is generally the case in microfluidic systems, e.g., water-oil emulsions.

Surface patterning of thin-layer electrode is widely used in microfluidic chips; however, it is not easy to fabricate two parallel electrodes on the opposite sides of a microchannel, as multilayer bonding is almost inevitable. In order to solve this problem, we employ a multistage process, depicted in Fig. 2, to fabricate the microfluidic chip with embedded parallel electrodes. Figure 2(a) shows the flow chart of the fabrication procedure, where the photolithography of a negative photoresist, SU8, is first used to fabricate a $50\text{-}\mu\text{m}$ -wide flow channel mold with height $h = 40\text{ }\mu\text{m}$. A positive photoresist, AZ4620, is then spin-coated on the mold and patterned by another photolithographic process to yield a cross sectional profile shown on the second row of Fig. 2(a). The thickness of AZ4620 should be larger than SU8, therefore triple coatings are needed, and the soft bake process is prolonged accordingly in order for the AZ4620 layer to reform a smooth surface. In the third step, cavities formed in the AZ4620 layer are filled with Ag + PDMS gel, which is a mixture of micro/nano Ag particles with PDMS gel. The cured Ag + PDMS composite has excellent electrical conductivity. [Tested conductivity is above $4 \times 10^4 (\text{S} \cdot \text{m}^{-1})$.²²] After baking at $60\text{ }^\circ\text{C}$ for 30 min and curing of Ag+PDMS, the remaining AZ4620 is dissolved in acetone and then the mold is gently washed in ethanol and DI water. The mold is then baked at $60\text{ }^\circ\text{C}$ for 20 min to evaporate the remaining organic solvent. In order to easily separate PDMS layer from mold, a nonstick thin film should be first deposited on the mold by evaporating silane in a desiccator. In the fourth step, PDMS gel is poured on the mold and then cured. After releasing, a cured PDMS layer is formed with conductive Ag+PDMS electrodes on two sides of the microchannel (shown as the fifth step). The cover layer of the chip is a sheet of

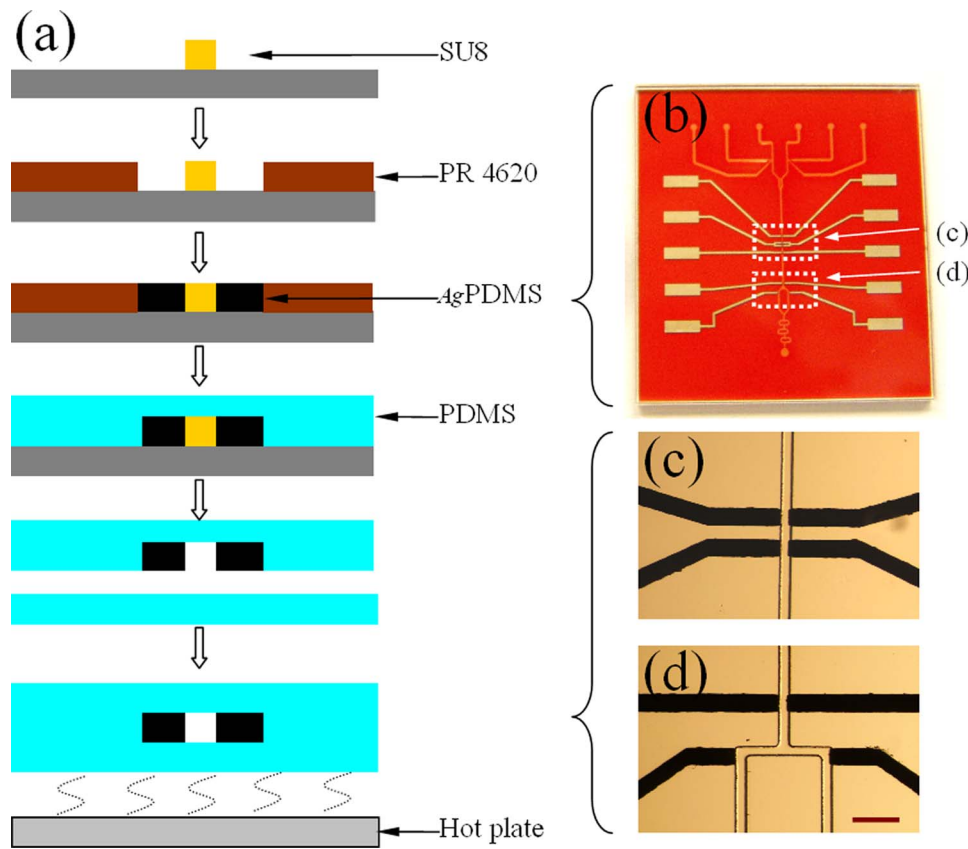


FIG. 2. (a) Processing flow of microfluidic chip fabrication using soft lithography. (b) An optical image of the channel mold and conductive components. (c) and (d) are optical images of the droplet detection area and directional flow control area, captured with an inverted microscope. Scale bar in (d): 200 μm .

PDMS. However, a patterned ITO glass can also be used as the cover, bonded to the channel layer with O_2 plasma treatment. A final one-hour baking at 150 $^\circ\text{C}$ is needed to stabilize the conductivity of the Ag+PDMS electrodes and the connecting lines. Figure 2(b) shows the optical image of the chip after the third fabrication step. Enlarged views of the detection and sorting areas are shown in Figs. 2(c) and 2(d), respectively.

B. Testing mechanism and circuit design

To form droplets in microchannels, the carrying fluid should preferentially wet the channel wall and the interfacial tension between the droplet phase and the carrying fluid should be lower than that between the droplet phase and the channel wall. Once the droplet is formed, the droplet will flow downstream encapsulated by a layer of the carrying fluid. The most commonly used carrying fluid is either silicone oil, hexadecane, or perfluorinated liquid, all electrically insulating with relatively low dielectric constants (compared to water). In our experiments, we employ aqueous droplets in silicone oil. Since the PDMS channel wall can be easily wetted by silicone oil, the two parallel electrodes cannot be electrically shorted by the aqueous droplets/plugs, verifiable through resistance measurements using an impedance analyzer.

An experimental setup, shown in Fig. 3(a), was built to test our capacitive detection scheme. The microfluidic chip was mounted directly on the circuit board [Fig. 3(b)], together with a syringe pump (Kdscientific) used to push different liquids into the chip. An electric shield (not shown in the picture) for the whole chip, as well as shielded electric lines for high voltage control were employed so as to minimize noise and signal loss. Capacitance signals were collected by a

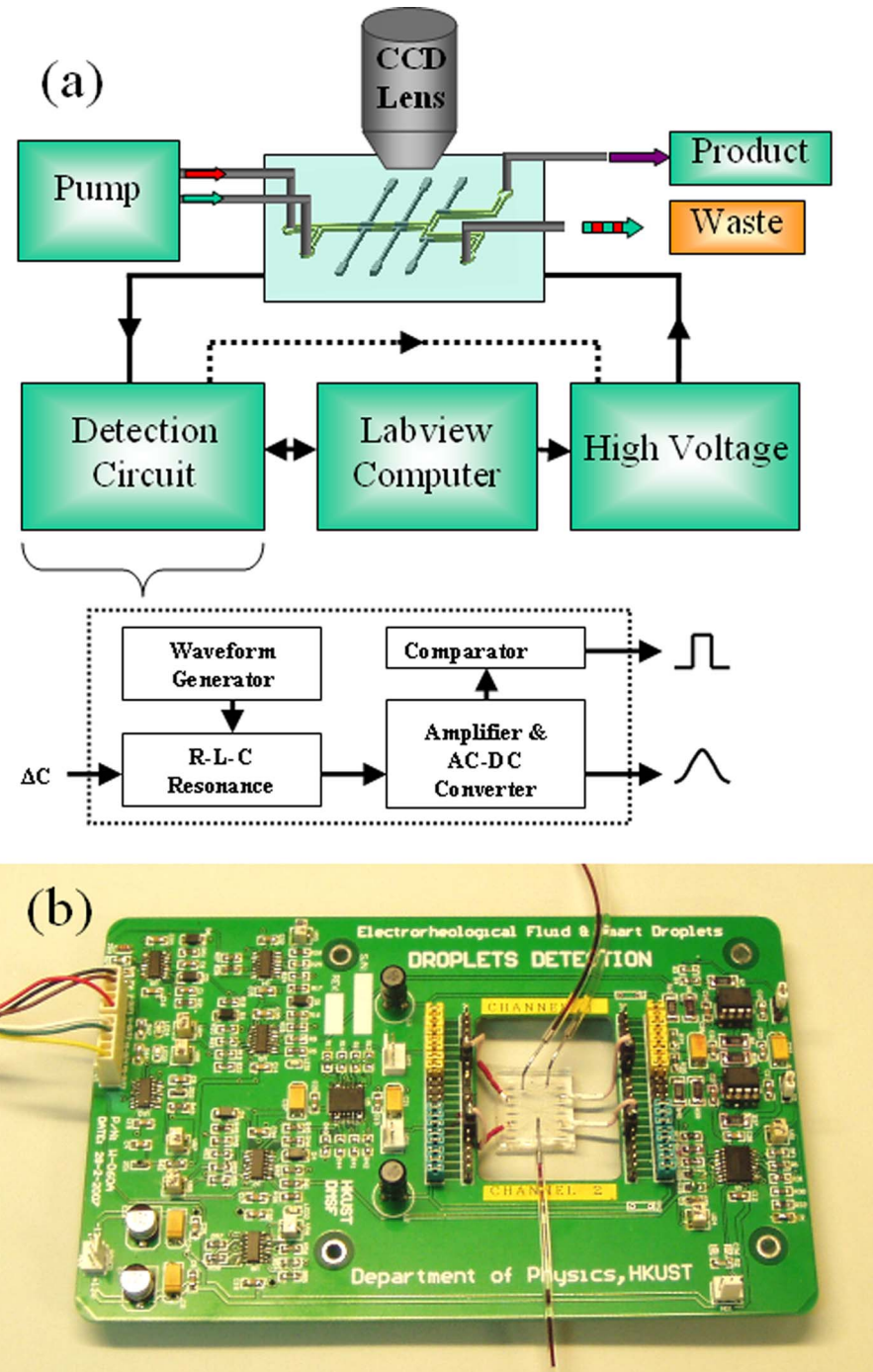


FIG. 3. (a) Schematics of the experimental setup for droplet detection and control. The detection circuit is composed of four parts as depicted in the dashed frame. (b) Optical image of the circuit board and the mounted chip for droplet detection.

Labview card. The Labview program can further drive high voltage switches to output control signals for droplet sorting. The detection circuit board with the chip shown in Fig. 3(b) was mounted on the platform of a microscope (Olympus X71). A high speed CCD camera (PCO. 1200s) was used to record the images for comparison and checking.

Detection circuit board is based on the resonance mechanism and consists of four parts, shown

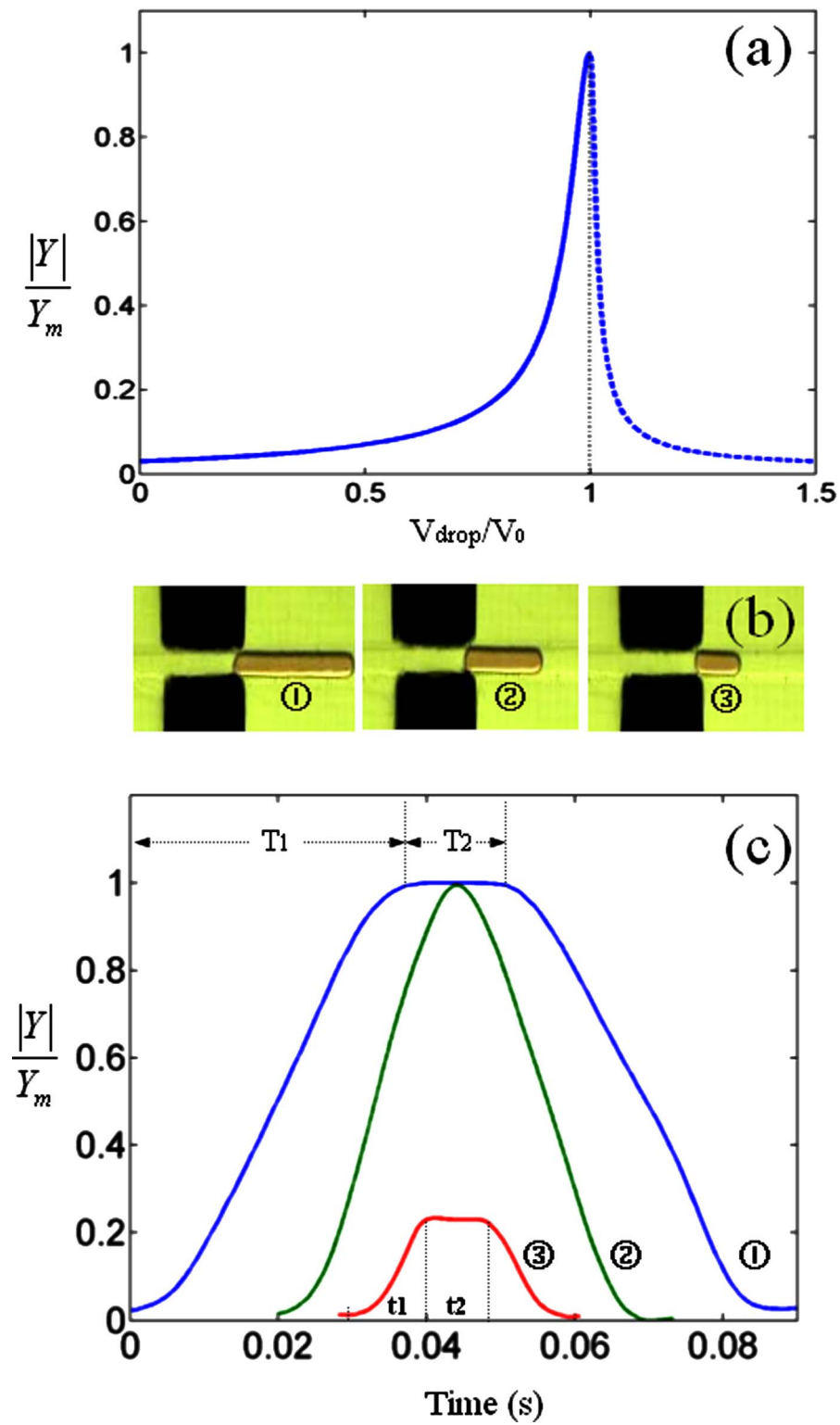


FIG. 4. (a) Relative amplitude of the voltage signal versus droplet volume. (b) Micrographs of droplets with lengths that are larger (case 1), equal (case 2), and smaller (case 3) than the electrode width. (c) Detected capacitive signals corresponding to the three droplets shown in (b).

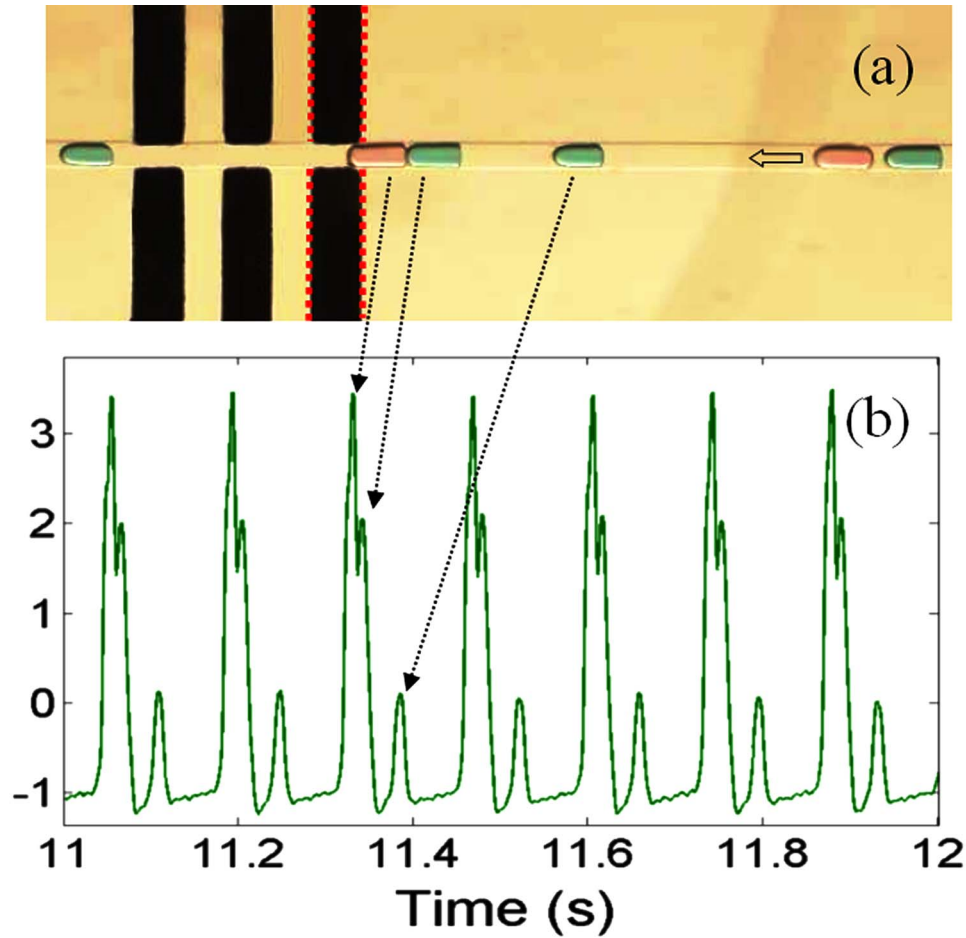


FIG. 5. (a) Optical image of a group of DI water droplets with different sizes. Small amount of dyes (without causing detectable variation of the dielectric constant for the droplets) was added for labeling. The detected signals are depicted in (b).

in the lower part of Fig. 3(a): an ac waveform generator that can output waveform with adjustable amplitude and frequency; a L - C resonance circuit where the capacitor C comes from the parallel electrodes in the chip; an amplifier and an ac-dc converter that output voltage peaks to correspond with the passing droplets; a supplementary comparator is included to output square wave signals for *in situ* feedback control of the droplets.

III. RESULTS AND DISCUSSION

A. Single droplet scanning

For the R - L - C resonance circuit, the voltage amplitude Y on the inductor is given by

$$|Y| = Y_m / [1 + (\omega L - 1/\omega C)^2 / R^2]^{1/2}, \quad (1)$$

where ω is the angular frequency and Y_m denotes the maximum amplitude of Y . When a water droplet passes through the electrodes, dielectric constant of the media between the electrodes changes as

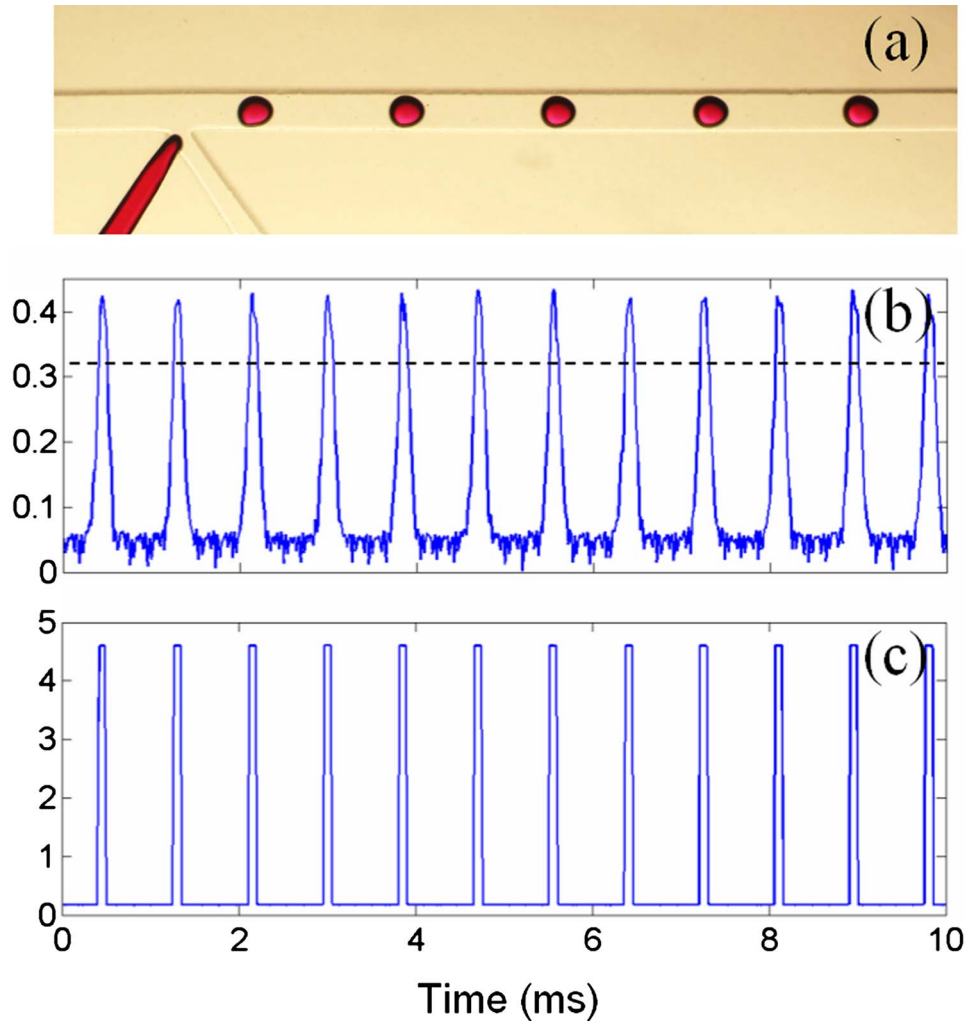


FIG. 6. (a) Optical image of a train of droplets generated in a flow focusing channel. (b) Detected signals. The dashed line denotes the threshold voltage of the comparator. (c) Square wave signals generated by the comparator that can be used directly for droplet control.

$$\varepsilon(t) = \varepsilon_{\text{oil}} + (\varepsilon_{\text{water}} - \varepsilon_{\text{oil}})V/V_0,$$

where V is the volume of water between the electrodes and V_0 is the total volume of the fluids between the electrodes. Correspondingly, capacitance varies as

$$C(t) = C_{\text{oil}} + (C_{\text{water}} - C_{\text{oil}})V/V_0.$$

C_{oil} denotes the capacitance when all of the media is oil, C_{water} denotes the capacitance when all of the media is water. By using an impedance analyzer (HP4192A), we have tested the capacitance rise to be 0.08 pF when a long DI water droplet fills the gap between the electrodes. The parasitic capacitance of the circuit was measured to be ~ 0.35 pF. By adjusting the resonance frequency to that when the parallel electrodes is filled with water, then the relationship of $|Y|/Y_m$ to the ratio V/V_0 of droplet volume V to the volume V_0 between the electrodes can be depicted as the solid line in Fig. 4(a), in accordance with Eq. (1). It is noted that the relationship is nonlinear, therefore the droplet size calibration is not as straightforward as a linear relationship, but the tested signals are highly selective in accordance to the volume of the droplet. Hence the detected signals can be used in droplet sorting—a small change in volume can result in a relatively large change in the

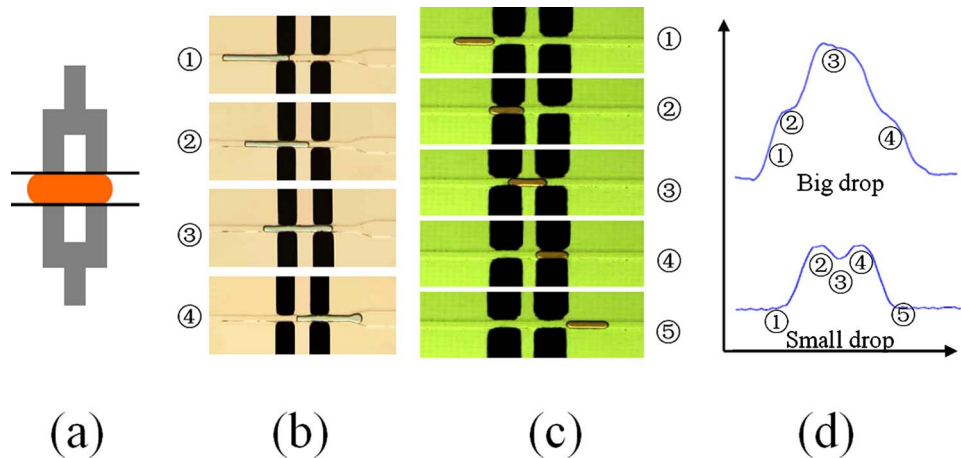


FIG. 7. (a) Schematic illustration showing the fork-shaped electrodes for droplet size and velocity detection. (b) and (c) are the optical images for big and small droplets passing through fork-shaped electrodes, respectively. The detected voltage signals are depicted in (d), and are marked according to droplets' positions in (b) and (c).

signal, especially if the signal is close to the peak value. The sharpness of the peak can be evaluated by the quality factor $Q_0 = 1/\omega_0 CR$. Figure 4(b) shows three snapshots of three separate droplets with different lengths passing through the electrodes. With flow rate being the same for the three cases, detected signals are displayed in Fig. 4(c). For case 1 where the droplet length L_d is larger than that of electrode, L_e , the velocity of the droplet can be deduced by $v = L_e/T_1$, while the length of droplet is $L_d = v(T_1 + T_2)$. However, for case 3 where the droplet length $L_d < L_e$, the velocity of the droplet is given by $v = L_e/(t_1 + t_2)$, with $L_d = vt_1$. Here T_1 , T_2 , t_1 , and t_2 are all defined in Fig. 4(c). It is noted that the testing results shown in Fig. 4(c) are approximately symmetric, corresponding to droplets with well-developed shapes and profiles. However, if a droplet has a nonuniform profile, e.g., caused by surface charge or flow asymmetry, its scanned signal can display an asymmetric waveform. Figure 5 gives a snapshot of a series of droplets with different sizes (upper panel), together with their corresponding scanned signals (lower panel). We have also calibrated the correlation of the detected signal magnitude with the droplet size to be 96%. The detection rate can reach up to $f_0/3$ droplets/sec., where $f_0 = 900$ kHz in our experiment. In our tests, we have detected at 1100 Hz, as shown in Fig. 6(a) for the actual droplets and the corresponding signals shown in Fig. 6(b). Here the limitation is not the detection rate, but rather the sustainable pressure for our PDMS chip (above which the chip breaks from the inlets ports). Figure 6(c) depicts square waveform output from the comparator for the feedback control that was introduced in Sec. II A.

B. Simplified electrode structure for droplet size and speed detection

From Fig. 4(c), it is seen that similar output signal waveforms were observed for both big and small droplets. The only difference is in their amplitudes. To measure the droplet size, two pairs of electrodes are needed, by which the velocity can be deduced directly by evaluating the time interval of the droplet passing from one pair of electrodes to the next. In Fig. 7(a) we show that a single pair of *fork-shaped* electrodes can perform the same task. When a droplet passes through a fork-shape electrodes [Figs. 7(b) and 7(c)], it is seen that corresponding to the consecutive time images of the big [Fig. 7(b)] and small [Fig. 7(c)] droplets passing through the fork electrodes, two plateau regions would appear on the scanned waveform as shown in Fig. 7(d) for the two cases. But the two waveforms are very different. For a big droplet with $L_d > L_e$, a peak in the middle can be identified; but for the small droplet with $L_d < L_e$, a dip appears. Hence the droplet size and velocity can be easily detected simultaneously with only one pair of fork-shaped electrodes.

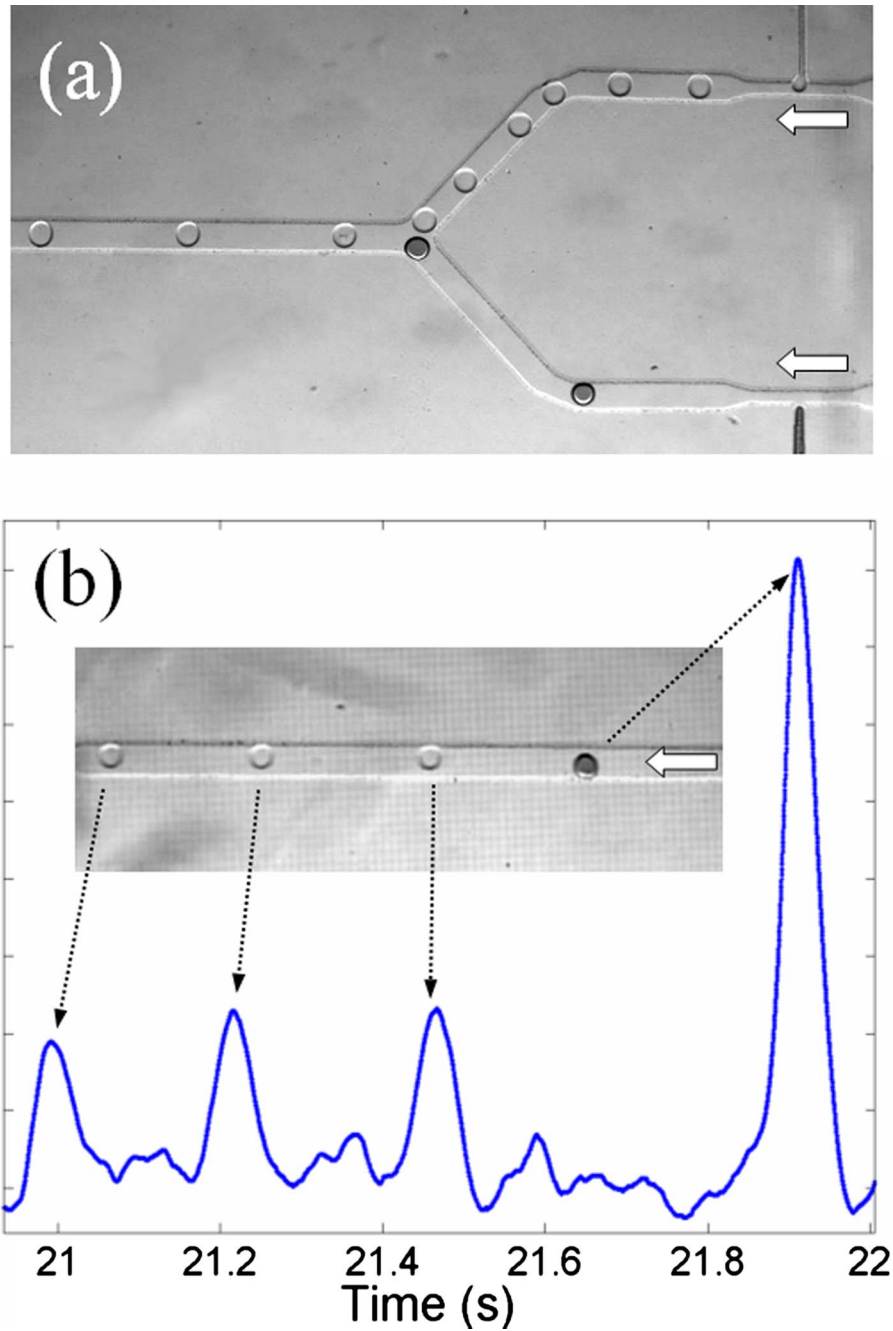


FIG. 8. (a) Image of a fork branch to separate droplets of the same size but different composition. (b) Detected signals with arrows pointing to the corresponding droplets.

C. Droplet composition detection

Because the chemical composition of the reagent(s) is related directly to the dielectric constant of the droplets, the capacitance and resonance caused by different droplet compositions can give rise to significantly different signal amplitudes. To test our experimental setup for detecting droplets with different dielectric constants, water and ethylene glycol were used as reagents, with dielectric constant of 80 and 37, respectively, at 20 °C. Two T-channels were applied to generate

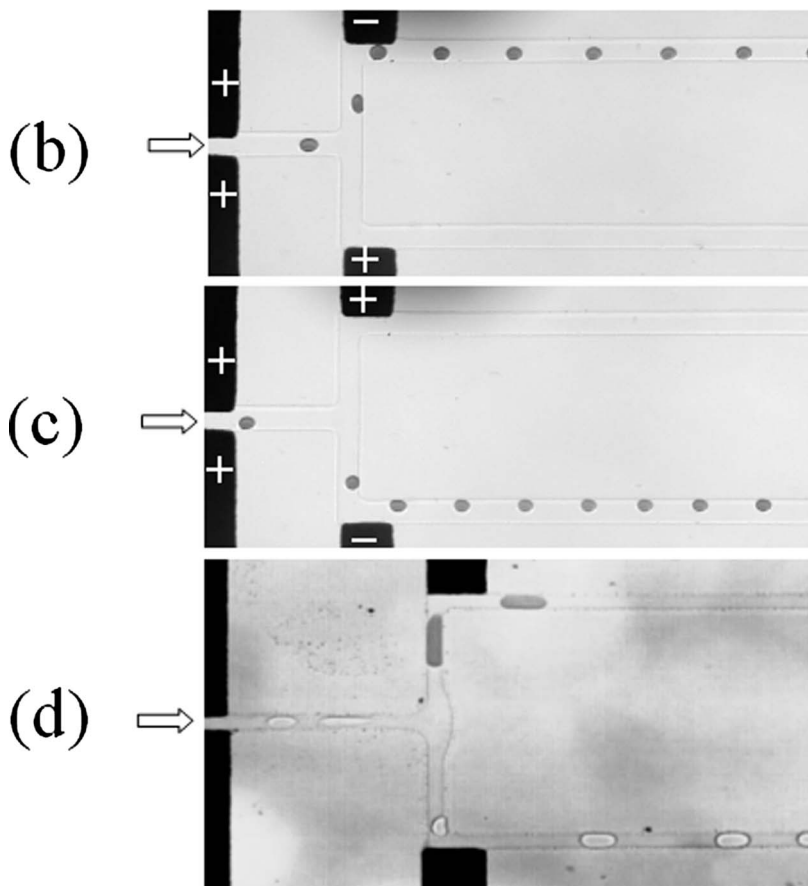
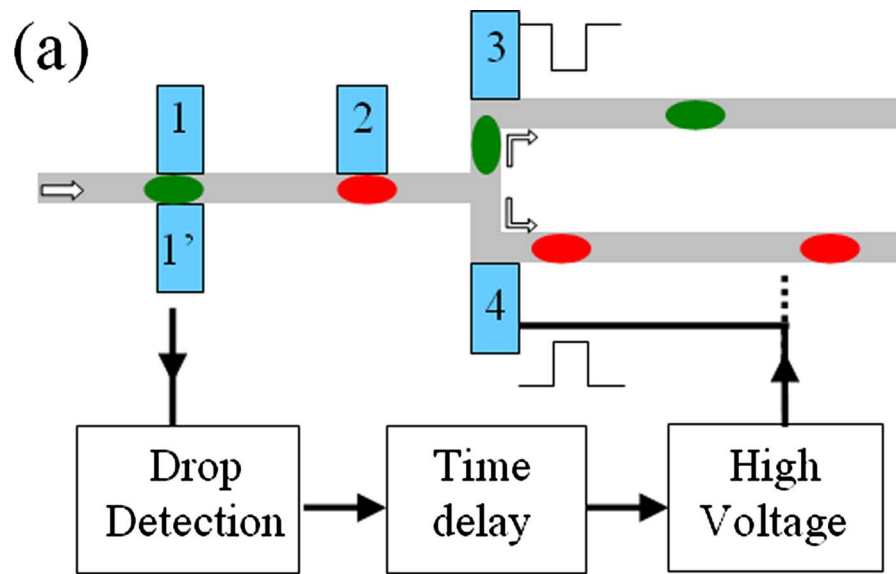


FIG. 9. (a) Flow chart of the feedback control circuit for droplet control. (b) and (c) Images showing the deflection of the droplets to either the upper or lower branch. (d) Image showing droplet sorting. All the water droplets are directed to the upper branch, whereas the light-colored ethylene glycol droplets are directed to the lower branch.

droplets with similar size by controlling the mass flow rate with two syringe pumps as shown in Fig. 8(a). The DI water (dark) and ethylene glycol (light) droplets are seen to give very different signal amplitudes, seen in Fig. 8(b).

D. Directional flow control of droplets

Droplet control and sorting according to size and content is a challenging but important task in microfluidics.^{23–26} Weitz²⁶ reported the fusion of droplets with different electrical charges, with directional flow control of the droplets from feedback of light detection. From our testing experiments described above, the capacitive signals in our approach can be used directly in the real-time manipulation of droplets in accordance with their size and content. Figure 9(a) shows schematically the feedback loop for the directional flow control of droplets. Velocity, size and/or content of the droplets were first determined with electrode 1-1'. The delay time for the droplet to reach the subsequent control electrodes is automatically adjusted in accordance with the velocity and channel length. Electrode 2 is connected to a high voltage with positive potential, while the polarizations of electrodes 3 and 4 are determined by the output signal of electrode 1-1'. For example, when a droplet arrives at the “T” intersection, it can be either attracted or repelled into one of the two branches, depending on the polarization of electrodes 3 and 4, as seen in Figs. 9(b) and 9(c). If electrode 4 is charged positive, the droplets will turn to the upper channel as can be seen in Fig. 9(b). The opposite situation is noted in Fig. 9(c). The minimum required effective electric field, E , for directional flow control is 400 V/mm, set by the hydrodynamic flow resistance at the T junction. For $E > 1100$ V/mm, the water droplets are stretched into tiny satellite droplets. Figure 9(d) shows a snapshot of droplet sorting according to composition. Here dark drops denotes water droplets, while light drops are ethylene glycol.

IV. CONCLUDING REMARKS

We present capacitive detection of microfluidic droplets based on the dielectric constant contrast between the droplets and the carrying fluid. Such detection is very sensitive, accurate and fast, and needs no special sample preparation. The tested capacitance signals can be used directly for *in situ* labeling, sorting and droplet manipulation. Therefore, this approach can be used in portable lab-chips for environmental monitoring and biofunctionalities, as well as in high throughput microchemical reactions and digital microfluidics.

ACKNOWLEDGMENTS

We would like to acknowledge, with appreciation, the support of Hong Kong Research Grant RGC HKUST-621006 for this work.

- ¹T. Thorsen, R. W. Roberts, F. H. Arnold, and S. R. Quake, *Phys. Rev. Lett.* **86**, 4163 (2001).
- ²H. Song, D. L. Chen, and R. F. Ismagilov, *Angew. Chem., Int. Ed.* **45**, 7336 (2006).
- ³A. J. deMello, *Nature (London)* **442**, 394 (2006).
- ⁴A. R. Wheeler, H. Moon H, C. A. Bird, R. R. O. Loo, C. J. Kim, J. A. Loo, and R. L. Garrell, *Anal. Chem.* **77**, 534 (2005).
- ⁵L. F. Cheow, L. Yobas, and D. L. Kwong, *Appl. Phys. Lett.* **90**, 054107 (2007).
- ⁶H. Song, M. R. Bringer, J. D. Tice, C. J. Gerdtts, and R. F. Ismagilov, *Appl. Phys. Lett.* **83**, 4664 (2003).
- ⁷P. B. Umbanhowar, V. Prasad, and D. A. Weitz, *Langmuir* **16**, 347 (2000).
- ⁸X. Zhang and K. Y. Chan, *Chem. Mater.* **15**, 451 (2003).
- ⁹M. J. Fuerstman, P. Garstecki, and G. M. Whitesides, *Science* **315**, 828 (2007).
- ¹⁰H. Willaime, V. Barbier, L. Kloul, S. Maine, and P. Tabeling, *Phys. Rev. Lett.* **96**, 054501 (2006).
- ¹¹L. H. Hung, K. M. Choi, W. Y. Tseng, Y. C. Tan, K. J. Shea, and A. P. Lee, *Lab Chip* **6**, 174 (2006).
- ¹²M. Y. He, J. S. Kuo, and D. T. Chiu, *Appl. Phys. Lett.* **87**, 031916 (2005).
- ¹³P. Guillot and A. Colin, *Phys. Rev. E* **72**, 066301 (2005).
- ¹⁴M. A. Schwarz and P. C. Hauser, **1**, 1 (2001).
- ¹⁵N. T. Nguyen, S. Lassemono, and F. A. Chollet, *Sensor Actuat., Biol. Chem.* **117**, 431 (2006).
- ¹⁶W. P. Eaton and J. H. Smith, *Smart Mater. Struct.* **6**, 530 (1997).
- ¹⁷C. Berggren, B. Bjarnason, and G. Johansson, *Electroanalysis* **13**, 173 (2001).
- ¹⁸D. K. Wood, S. H. Oh, S. H. Lee, H. T. Soh, and A. N. Cleland, *Appl. Phys. Lett.* **87**, 184106 (2005).
- ¹⁹G. Marchand, C. Delattre, R. Campagnolo, P. Pouteau, and F. Ginot, *Anal. Chem.* **77**, 5189 (2005).

- ²⁰G.A. Ferrier, A.N. Hladjo, D.J. Thomson, G.E. Bridges, M. Hedayatipoor, S. Olson and M. Freeman, *NSTI Nanotech* (2007).
- ²¹L. L. Sohn, O. A. Saleh, G. R. Facer, A. J. Beavis, R. S. Allan, and D. A. Notterman, *Proc. Natl. Acad. Sci. U.S.A.* **97**, 10687 (2000).
- ²²X. Z. Niu, S. L. Peng, L. Y. Liu, W. J. Wen, and P. Sheng, *Adv. Mater.* **19**, 2682 (2007).
- ²³G. Cristobal, J. P. Benoit, M. Joanicot, and A. Ajdari, *Appl. Phys. Lett.* **89**, 034104 (2006).
- ²⁴C. Priest, S. Herminghaus, and R. Seemann, *Appl. Phys. Lett.* **89**, 134101 (2006).
- ²⁵K. Ahn, J. Agresti, H. Chong, M. Marquez, and D. A. Weitz, *Appl. Phys. Lett.* **88**, 264105 (2006).
- ²⁶D. R. Link, E. Grasland-Mongrain, A. Duri, F. Sarrazin, Z. D. Cheng, G. Cristobal, M. Marquez, and D. A. Weitz, *Angew. Chem., Int. Ed.* **45**, 2556 (2006).